34. SOME HIGHLIGHTS OF RECENT V/STOL AERODYNAMICS RESEARCH

By John P. Campbell
NASA Langley Research Center

SUMMARY

Some of the highlights of the papers on aerodynamics research in the recent NASA Conference on V/STOL and STOL Aircraft are presented. The V/STOL types discussed include helicopters, propeller V/STOL, lift-fan and cruise-fan V/STOL, and jet-lift V/STOL.

INTRODUCTION

This paper presents some of the highlights of the papers which dealt with aerodynamics in the NASA Conference on V/STOL and STOL Aircraft held at the Ames Research Center on April 4-5, 1966. It covers research reported in the three sessions: Helicopters and Propeller V/STOL, Lift-Fan and Cruise-Fan V/STOL, and Jet-Lift V/STOL. The paper is not intended to be a general state-of-the-art summary of V/STOL aerodynamics research but is merely a presentation of some of the highlights of the conference. No attempt is made to cite the individual sources of the material presented herein, but the reader may find these sources by referring to reference 1.

SYMBOLS

A propeller disk area, sq ft

A_j jet nozzle area, sq ft

b wing span, ft

$C_{D,W}$ wave-drag coefficient based on frontal area

C_f effective skin-friction coefficient

C_L lift coefficient

$C_{T,s}$ thrust coefficient, $T/q_s A$

D propeller diameter, ft; jet-engine tailpipe diameter, ft

D drag, lb

D_e equivalent diameter; diameter of a single nozzle having the same area as the sum of the several nozzles of a multijet configuration, ft

EGT   exhaust-gas temperature, $^\circ F$

e span efficiency factor

h height of model above ground, ft

i_d duct incidence angle, deg

L lift, lb

ΔL incremental lift

ΔL_b incremental lift due to base loss, lb

ΔL_w increment in wing lift, lb

M Mach number

ΔM increment in pitching moment due to interference, ft-lb

q_n dynamic pressure at nozzle exit, lb/sq ft

q_s slipstream dynamic pressure, lb/sq ft

q_x dynamic pressure at distance x downstream of nozzle, lb/sq ft

R rotor radius, ft

$\dot{r}_{max}$ maximum self-generated yaw disturbance, deg/sec^2

S total planform area, sq ft

S_{wet} wetted area, sq ft

T thrust, lb

T_I ideal jet thrust, lb

T_s static thrust, lb

V free-stream velocity, ft/sec or knots

V_j jet velocity, ft/sec

$V/\Omega R$ advance ratio

V_∞	free-stream velocity, ft/sec
W	gross weight, lb
x	distance downstream from jet exit, ft
α	angle of attack, deg
β_V	lift-fan vector angle from fan axis, deg
γ	flight-path angle, deg
δ_f	flap deflection, deg
θ_j	jet deflection, positive downward from chord line, deg
ρ_j	air density in jet, slugs/ft^3
ρ_∞	free-stream air density, slugs/ft^3
Ω	rotor angular velocity, rad/sec

HELICOPTERS AND PROPELLER V/STOL

For helicopters, information is presented on two promising rotary-wing concepts - the hingeless rotor and the jet-flap rotor; some recent research dealing with descent capability and slipstream recirculation for the tilt-wing V/STOL type is discussed.

Hingeless Rotor

Figure 1 presents relative damping moment and control moment in hovering calculated for three helicopter types - one having a rotor with a central hinge, one having a rotor with the flapping hinge offset 4 percent of the rotor radius, and one having a hingeless rotor. The solid lines are for sea level and the dashed lines for an altitude of 15 000 feet. The damping and control moments are referenced to the values for the rotor with the central hinge at sea level. Moving up the lines for the other two rotor types represents increasing the rotor blade weight. The data show that incorporating hinge offset provides increases in both damping and control moment over the values for the rotor with the central hinge, and the use of the hingeless rotor provides even greater increases. There is a limiting upper boundary for the hingeless rotor labeled "Unacceptable gyroscopic coupling." If rotor weight is increased to the point where this boundary is crossed, excessive coupling of rolling and pitching motions will be experienced. Increasing altitude from sea level to 15 000 feet causes a substantial increase in relative damping for all three rotors and also

a reduction in control moment for the hingeless rotor. An important point to be brought out here is that a hingeless rotor design which is on the satisfactory side of the coupling boundary at sea level may move to the unsatisfactory side when operating at altitude. To reduce the coupling at altitude it may be necessary to use lighter blades in order to move down on the curve below the boundary, or it may be possible to minimize the coupling by the use of some feedback device.

Jet-Flap Rotor

The jet-flap rotor has been proposed as a means of delaying retreating blade stall and thereby permitting much higher forward speeds for the helicopter. Figure 2 shows cross-section views of the blade of a jet-flap rotor recently tested at Ames in the 40- by 80-foot tunnel. The rotor was built by the French firm of Giravions Dorand under contract to the U.S. Army. It is driven by compressed air which is ducted through the blade spar and exhausted in a thin sheet over a trailing-edge flap which extends over the outboard third of the blade radius. Deflection of the jet flap is used for cyclic and total pitch control.

The capability of the jet-flap rotor on the basis of tests to date compared with that for a conventional rotor is shown in figure 3. Values of lift for both rotors ratioed to the static thrust of the conventional rotor are plotted against airspeed. Over the speed range covered in the tests, the measured values for the jet-flap rotor are well above the upper limit of lift capability for conventional rotors as determined from blade stall limitations. The top speed in the jet-flap rotor tests was established by a mechanical limitation on flap deflection to about $50°$ on the test rotor. Since there were no indications of retreating blade stall at this speed, it appears likely that substantially higher speeds could be obtained on a modified rotor. The experimental data and calculations (based on the method of ref. 2) for the jet-flap rotor show the same general trends where they can be compared; but in the highest speed range, the calculations involve a number of uncertainties and may prove to be somewhat optimistic. In any event, the results obtained to date with the jet-flap rotor indicate a promise of higher forward speeds for the helicopter.

Propeller V/STOL

Propeller tilt-wing V/STOL aircraft experience a limitation on descent capability because of wing stall during partial-power descent conditions when the slipstream velocity is low. Considerable research has been carried out in this area and results have indicated that the problem is quite amenable to solution by careful design. Some of the more recent research on the problem has been carried out with the model shown in figure 4. This large-scale semi-span research model is being used in systematic studies of configuration variables in the Langley full-scale tunnel. One of the important variables in determining partial-power descent capability is the vertical position of the propeller thrust line. Some results obtained with this model on the effect of

propeller position are shown in figure 5. Flight-path angle γ (positive for climb and negative for descent) is plotted against thrust coefficient $C_{T,s}$. A value for $C_{T,s}$ of 1.0 represents hovering and values from about 0.6 to 0.9 generally cover the transition range. Wing stall boundaries are shown for three vertical positions of the propeller with respect to the wing. The data show that moving the propeller from a high to a low position results in the capability for descending at much steeper angles without wing stalling. The XC-142 tilt-wing airplane, which has a propeller position corresponding to the mid position shown in figure 5, has operated satisfactorily at descent angles up to 15°.

A problem that has proved more bothersome than descent capability for the XC-142 is the effect of slipstream recirculation in ground effect. Figure 6 presents some information on this problem. The sketch at the right of the figure illustrates the type of flow developed around the airplane as it approaches the ground at very low speeds. Some of the propeller slipstream moves forward after striking the ground and recirculates to create a turbulent region through which the airplane must fly. The airplane experiences disturbances about all axes, but, for the XC-142, the yaw disturbances seem to predominate and give the most trouble. The plot at the left shows yaw disturbances in terms of maximum yaw accelerations experienced by the XC-142 plotted against airspeed. The pilots of the airplane indicate that in the airspeed range from about 12 to 30 knots there is danger of losing control as a result of these disturbances. A crash landing of one of the airplanes in 1965 was attributed to this problem. Wind-tunnel and flight research has shown that varying the flap programing can reduce the range of wing incidence where the problem is encountered but the speed range of concern is not changed. At present, the problem is being avoided in flight by flying at speeds greater than 30 knots or less than 12 knots when in ground effect. Eventual solution of the problem may require increased control capability over that now available or some additional artificial stabilization.

LIFT-FAN AND CRUISE-FAN V/STOL

Tandem Lift Fan

Figure 7 shows a large-scale model of a tandem lift-fan configuration mounted for testing in the Ames 40- by 80-foot tunnel. This model has tandem lift fans fore and aft of the wing at the wing-fuselage juncture. Figure 8 shows the variation of lift with airspeed for this model. The lift is given in terms of the static thrust and the airspeed is given in terms of V/V_j where V_j is the jet velocity. Curves are shown for operation of rear fans only, front fans only, and all four fans. The rear fans induce a substantial increase in lift with increasing speed whereas the front fans induce negative lift. A small increase in lift occurs when all four fans are operating.

Lift-Cruise Fan

The lift-cruise fan configuration shown in figure 9 mounted for testing in the Ames 40- by 80-foot tunnel has lift fans mounted forward on the fuselage so they can be extended as shown for hovering and transition and can be folded into the fuselage for cruising flight. The fans at the rear are cruise fans which are mounted on pylons so that they can be rotated to a vertical position for hovering flight. The effect of the front fans on wing lift is shown in figure 10. The ratio of wing lift to fan static thrust is plotted against velocity ratio for three positions of the front fans. A loss in lift due to fan operation occurs for all fan positions, the greatest loss being obtained in position 1, directly ahead of the wing, and the least loss being obtained in position 3, the low position. Despite this loss in wing lift due to fan operation, the net wing lift can be made positive by using sufficient wing camber and flap deflection. There is also a positive induced lift on the fan fairings. The ratio of total lift to static thrust for the model with the front fans in the low position is shown in figure 11 plotted against airspeed. For these tests, the wing flaps were set at 45° and the cruise fans were tilted at various angles so that the fan thrust balanced the drag. There appears to be a substantial increase in lift with increasing speed which would indicate considerable STOL capability. However, this increase in lift or STOL capability is not nearly as great as it could be if the fan slipstream were spread out more or less uniformly across the span of the wing as is done in the case of V/STOL configurations such as the tilt wing.

This point is illustrated in figure 12 which compares the thrust required for level flight in the transition range for lift-cruise-fan and tilt-wing configurations having a wing loading of 100 pounds per square foot. The thrust is shown in terms of thrust-weight ratio. The more rapid dropoff in thrust required with increasing airspeed for the tilt wing is an indication of greater STOL capability. In addition, the curves indicate that in low-speed landing approaches the tilt wing could operate at lower thrust values, which is very desirable from the standpoint of fuel consumption.

Deflected-Slipstream Cruise Fan

The comparison shown in figure 12 indicates that it would be very desirable to develop V/STOL fan configurations having a more rapid dropoff in thrust required. Some exploratory research in this direction has recently been carried out at Langley Research Center with the configuration shown in figure 13. This configuration has four cruise fans spaced along the wing and blowing over a slotted flap. As shown by the cross-section sketch at the right of the figure, part of the flow goes over and part under the wing. The flow under the wing spreads out and blows through the slotted flap all across the span to induce a fairly uniform lift on the wing by means of the jet-flap principle. Some results of tests of a small-scale semispan model of this configuration are presented in figure 14 on a plot of thrust-weight ratio against airspeed. The curve for the lift-cruise fan is repeated for comparison. The data for the deflected-slipstream cruise-fan configuration look promising; in fact, the curve approaches the result which would be obtained with an elliptical load

502

distribution across the entire span of the wing. Only a limited amount of research has been done on this concept to date, however, and an evaluation is premature until more is known of the problems. One obvious problem of such a configuration is the very large nose-down pitching moment which must be trimmed by some auxiliary device in hovering and low-speed flight. The important point to be brought out here is that it does appear possible to get high induced wing lift and good STOL capability with fan configurations. This is an area warranting special attention in future research.

JET-LIFT V/STOL

Cruise Performance

One of the papers in the jet V/STOL session of the NASA V/STOL and STOL Conference summarized some of the design principles now being used for cruise optimization of conventional aircraft in order to illustrate potential improvements for V/STOL designs. Figures 15 and 16 taken from this paper compare the subsonic aerodynamic efficiency of conventional and V/STOL aircraft. Figure 15 presents values of $(L/D)_{max}$ plotted against the ratio of span to wetted area for fighter aircraft. The shaded region and circular symbols are for V/STOL aircraft (data primarily from design studies, since flight data on these aircraft are limited). The term C_f/e, effective skin-friction coefficient divided by span efficiency factor, is a correlating parameter represented by the straight line faired through the data points. It appears that the effective skin-friction level for V/STOL fighters is similar to that for conventional fighters but, because of the extra size required to house the lifting systems, the values of span-to-wetted-area ratio are lower for the V/STOL fighters and hence the values of $(L/D)_{max}$ are lower.

In figure 16, for bombers and transports, the V/STOL airplanes are seen to have higher effective skin friction as well as lower span-to-wetted-area ratios. The values of $(L/D)_{max}$, therefore, are much lower than those for the conventional aircraft. This correlation indicates the directions in which refinements are needed to increase the subsonic aerodynamic efficiency of V/STOL aircraft. That is, the effective skin friction should be reduced by greater cleanness, and the span-to-wetted-area ratios should be increased.

Figure 17 illustrates a point regarding the performance of supersonic configurations. One of the items that makes design of supersonic V/STOL aircraft more complicated than that for conventional aircraft is the volumetric constraint associated with having propulsive systems to provide lift as well as thrust. This point is illustrated in figure 17 which presents wave-drag coefficient, based on frontal area, plotted as a function of equivalent-body fineness ratio. The square symbols in the shaded area on the right are representative of conventional aircraft. The circular symbols are for V/STOL study configurations incorporating vectored-thrust engines. The diamond symbol represents a subsonic V/STOL aircraft. Because of the volumetric constraint, the V/STOL configurations utilizing vectored-thrust engines generally have

lower fineness ratios than the conventional aircraft and, therefore, have higher wave-drag coefficients. For V/STOL configurations using lift engines and separate cruise engines, it may be possible to increase the fineness ratio and provide somewhat lower wave drag in the region between the two bands.

Hovering Performance

Figure 18 shows the effect of jet arrangement on base loss and jet decay. The term "base loss" refers to the aerodynamic lift loss in hovering resulting from suction forces on the bottom of the airplane. Data are shown for single-jet, multijet, and multislot arrangements having the same total jet area. In the top plot, the ratio of lift loss to static thrust is plotted against the square root of the planform-to-jet-area ratio. In the bottom plot, q_x (the measured dynamic pressure at a distance x downstream) divided by q_n (the dynamic pressure at the nozzle exit) is plotted against the distance downstream in terms of the effective diameter. This figure shows that the lift loss is a function of the decay characteristics; that is, the more rapid the decay the larger the loss.

From the standpoint of base loss then, it would seem that a rapid decay rate is not desirable. However, from the ground erosion standpoint, a rapid decay of dynamic pressure is very desirable, and efforts are being made to devise means of achieving rapid decay with special nozzles. The Boeing Company has just completed a study for NASA to determine the effects of different nozzle arrangements on jet decay. Some of the results are shown in figure 19 which is a plot of dynamic-pressure ratio against distance downstream for a circular nozzle and for single-slot and four-slot nozzles. The slot nozzles appear to achieve the desired goal of rapid dynamic-pressure decay. The thrust losses for these nozzles measured at an x/D_e of 3 are shown in figure 20. The ratio of the loss to the ideal static thrust is plotted against the dynamic-pressure ratio for the nozzles of figure 19 along with the data for other multislot nozzles which have been investigated. It can be seen that the rapid decay of dynamic pressure comes at the expense of the basic nozzle efficiency. Also shown are the base losses measured with a fuselage in the presence of the suppressor nozzles. It is apparent from these results that the requirement for rapid decay of jet exhaust velocity to prevent ground erosion has to be carefully considered in light of the larger nozzle and base losses associated with suppressor nozzles.

Hot-Gas Ingestion

Hot-gas ingestion is a serious problem for jet V/STOL aircraft because the raised inlet air temperature can result in drastic thrust losses. Unfortunately, little systematic work has been done in this field, but research is now underway with large-scale models at both Ames Research Center and Langley Research Center to provide information on the subject. Figure 21 shows a sketch of the general research model at Langley Research Center which is powered by a single J-85 engine in the fuselage and can be fitted with various exhaust and

inlet arrangements. The lower sketch shows the hot-gas recirculation pattern for the model in a four-nozzle configuration. With this configuration, the hot gas, in addition to flowing outward along the ground in all directions, flows upward in a sort of fountain effect between the engines. There is also an upward flow fore-and-aft against the bottom of the fuselage as indicated by the short dashed lines. The hot gases in the upward and forward flows are of course quite accessible to the engine inlets and are still very hot because they have not traveled very far and little mixing with the ambient air has taken place.

The inlet temperature rise for this configuration is shown in figure 22 together with data from similar small-scale models tested by Bell and North American. The temperature rise is shown as a function of height above the ground in effective nozzle diameters. All three models were tested with side inlets and the Langley model was also tested with a single top inlet. The data show that both side and top inlets experienced very high temperatures near the ground, the model with the top inlet having the higher temperature. As nozzle height was increased, the temperature rise decreased rapidly, and at a height of 5 diameters the rise was of the order of 20° F. These very high temperatures occurred within 2 seconds following downward deflection of the exhaust nozzles. VTOL operation would not be possible with these high temperatures because of the high thrust loss and the probability of compressor stall.

One way of minimizing the fountain effect which apparently causes the high inlet temperatures is to arrange the exhaust nozzles in a line instead of in a rectangular pattern. Some tests of the Bell model in such a configuration showed a temperature rise of only 10° in the top inlet.

The effect of another important configuration parameter, wing position, is illustrated in figures 23 to 25 which present some results obtained with a large-scale Norair model tested at Ames Research Center. Figure 23 shows a sketch of the model which has five J-85 engines mounted vertically in the fuselage and two propulsion engines at the rear of the fuselage with the exhaust diverted downward for vertical lift. The inlet location of the propulsion engines could be varied and the wing was also tested in different positions. Figures 24 and 25 present results of tests for two different configurations of the model, one having high ingestion and one having low ingestion.

Figure 24 shows the case of high ingestion. The sketch on the left illustrates the recirculating flow pattern for the high-wing configuration. The flow along the ground from the lift engines meets the flow from the propulsion engines to produce an upward flow of hot gas which is ingested into the inlets. The plots at the right show that the temperature in the inlet of engine number 3 reached about 200° F in about 3 seconds after the engines were accelerated to full thrust. The engine then experienced a compressor stall.

Figure 25 shows results for a configuration for which there was very little ingestion. In this case, the wing is in a low position and obstructs the upward and forward flow of hot gas and causes it to recirculate below the wing as indicated by the arrows. The plots at the right indicate little or no ingestion in the inlet of engine 3 in this case. It appears therefore that wing position can be a very important factor in minimizing hot-gas ingestion. Perhaps some form

of extendible deflectors could be used to serve the same purpose as the low wing of this configuration.

In any event, the state of the art in this important area is still in the exploratory stage; and it appears that the development of jet V/STOL designs at this time should include hot-gas ingestion tests for the particular configuration and operating conditions that are expected to be encountered.

Transition Aerodynamics

Some jet-induced interference effects in transition for jet V/STOL aircraft are illustrated in figures 26 to 29. Figure 26 shows the effect of wing planform on jet-induced pitching moment and lift loss. Data for a swept and an unswept wing are plotted against an effective velocity ratio, where zero represents hovering and 0.25 represents the upper end of the transition range. Suction pressures on the bottom of the wing-fuselage combination produce a lift loss similar to that shown earlier for the lift-cruise fan configurations. The loss is about the same for the swept and unswept configurations. The nose-up pitching moment, however, is greater for the swept wing configuration because much of the area on which the suction pressures act is farther behind the center of gravity.

The arrangement of the jets can also have a large effect on the magnitude of the induced interference effects, as shown in figure 27. Data for a four-jet configuration are compared with data for a configuration in which the same total jet area is arranged in a central slot to represent a row of lift engines. It can be seen that changing from the rectangular to the linear arrangement gives a very large reduction in both the nose-up pitching moment and the lift loss.

The data shown in figures 26 and 27 are for tail-off configurations. In addition to the jet-induced suction pressures on the lower surfaces of the wing and fuselage, there is also a large induced downwash at the horizontal tail which causes an additional nose-up pitching moment. This downwash is a function of angle of attack and can therefore change both trim and stability. The effect of power on the tail contribution to stability is highly dependent on the flow field in which the tail operates and, in particular, on the flow field generated by the parts of the airplane ahead of the wing. Figures 28 and 29 illustrate this problem. Figure 28 represents an airplane in cruising flight. On most modern high-speed jet airplanes there are inlets or other elements such as fixed forewings for variable-sweep wings which produce lift and shed vortices inboard and it is generally considered desirable that the tail be located below this trailing vortex system. This arrangement causes the tail to move away from the vortices as the angle of attack is increased. For the jet VTOL airplane in transition flight, however, the situation is different, as shown in figure 29. The inboard vortices can be pulled below the horizontal tail by the action of the lifting jets. Then as the angle of attack is increased, the tail is forced to move through these vortices. The severity of the problem thus created depends on many configuration variables, such as the position and size of the forewing and engine inlets and the horizontal-tail configuration and tail

length. In general, the effects of large inlets located well forward have been found to be detrimental.

CONCLUSION

The subjects covered in this paper are covered in much more complete form in the compilation of papers from the NASA Conference on V/STOL and STOL Aircraft, available as NASA Special Publication, SP-116.

REFERENCES

1. Anon.: Conference on V/STOL and STOL Aircraft. NASA SP-116, 1966.

2. Evans, William T.; and McCloud, John L., III: Analytical Investigation of a Helicopter Rotor Driven and Controlled by a Jet Flap. NASA TN D-3028, 1965.

HELICOPTER CONTROL AND DAMPING

RELATIVE DAMPING MOMENT

UNACCEPTABLE GYROSCOPIC COUPLING

HINGELESS ROTOR

ALTITUDE, FT
——— 0
– – – 15 000

ROTOR WITH HINGE OFFSET

ROTOR WITH CENTRAL HINGE

RELATIVE CONTROL MOMENT

Figure 1

JET–FLAP ROTOR

NOZZLE

θ_j

V_j

MAIN AIR DUCT

NOZZLE

V_j
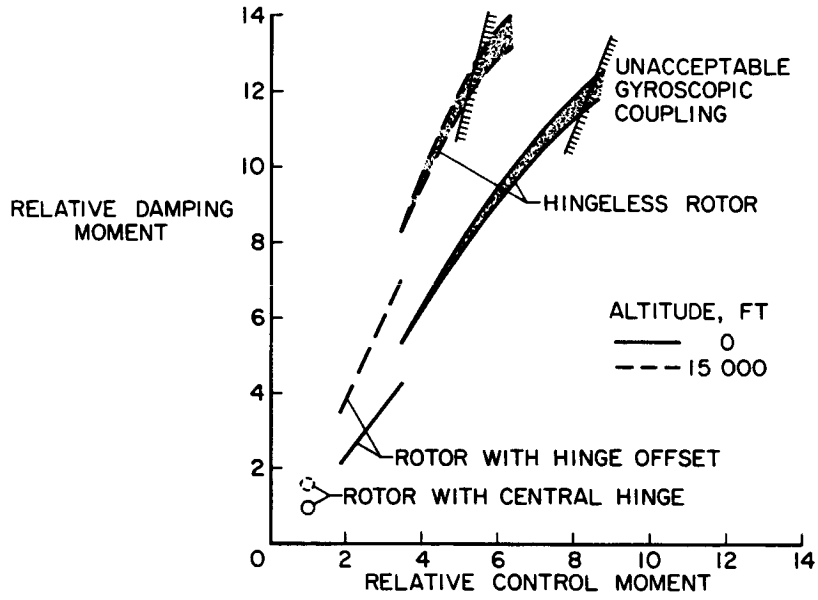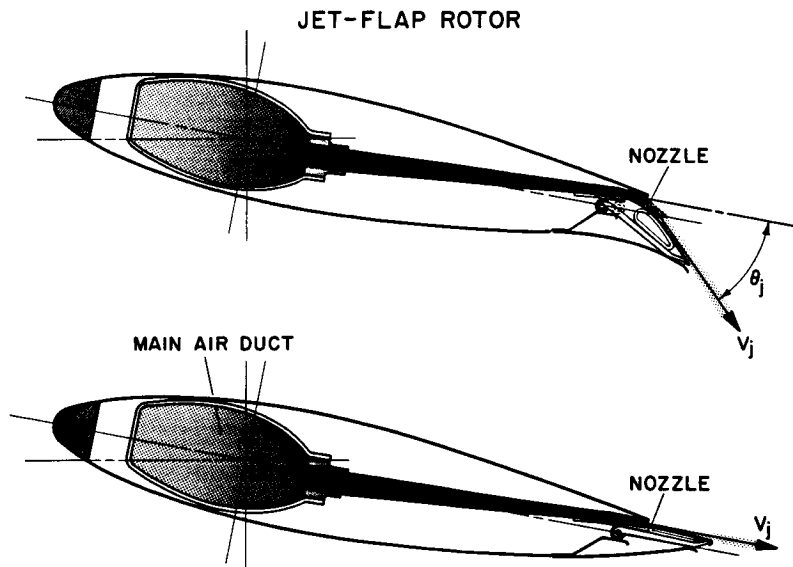
Figure 2

JET-FLAP ROTOR CAPABILITY
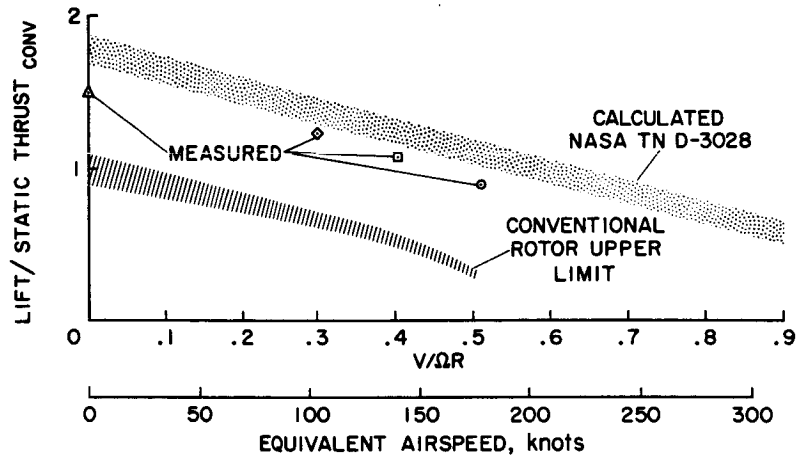
Figure 3

LARGE-SCALE TILT-WING MODEL
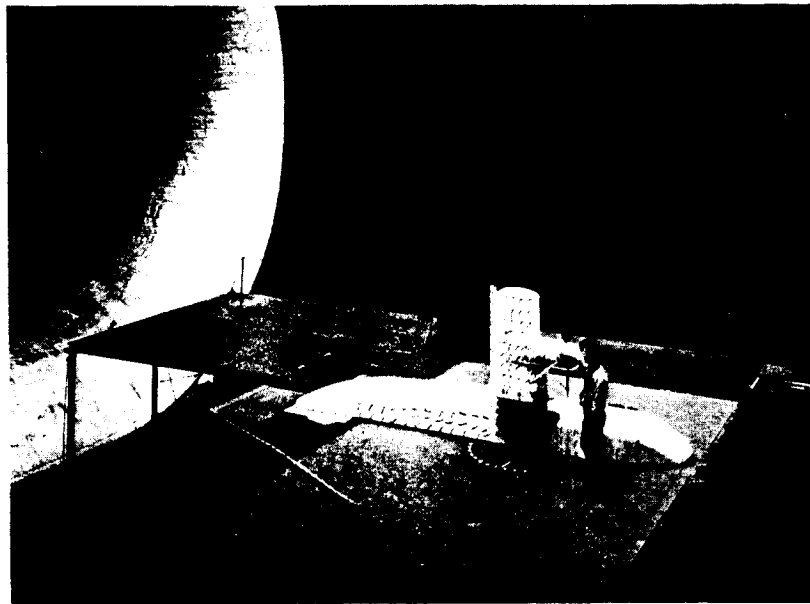
Figure 4   L-2698-6

EFFECT OF PROPELLER POSITION
DOWN-AT-CENTER ROTATION ; δ_f = 20°
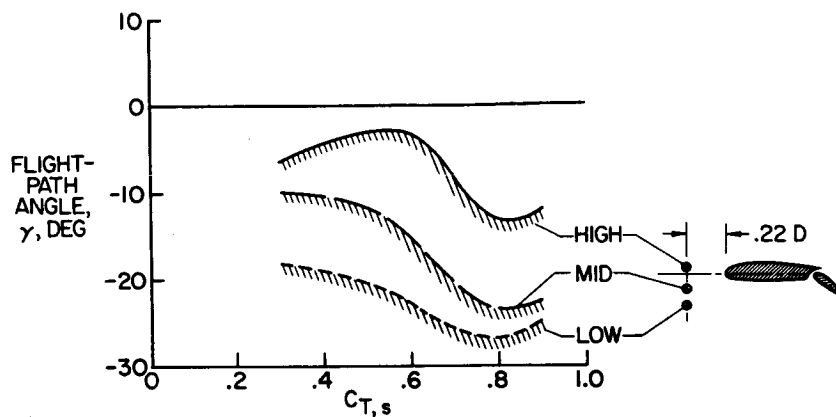
Figure 5

YAW DISTURBANCES IN GROUND EFFECT
TILT-WING AIRPLANE
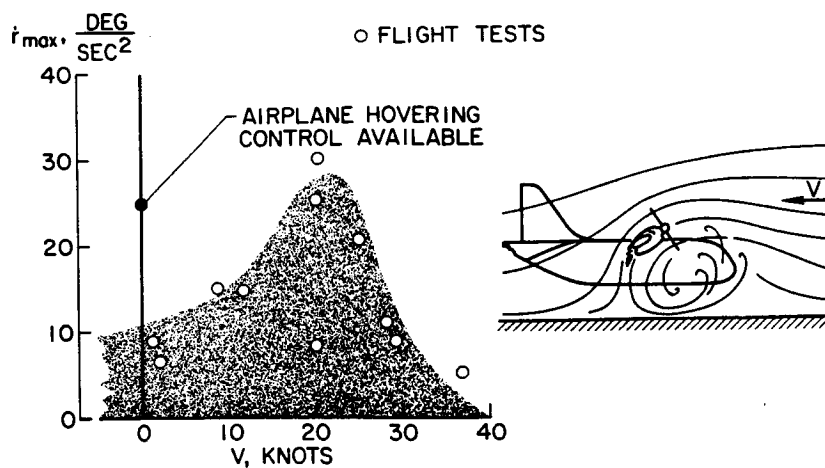
Figure 6

THE TANDEM LIFT-FAN MODEL
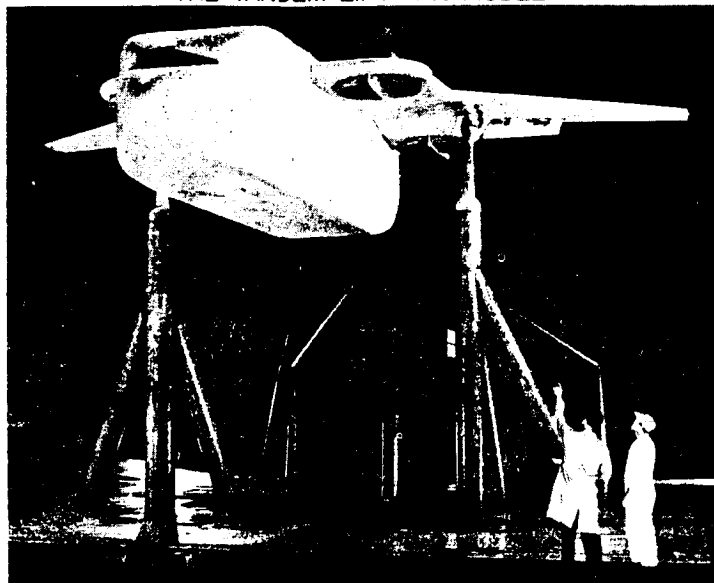
Figure 7   L-2698-10

VARIATION OF LIFT WITH AIRSPEED FOR THE
TANDEM LIFT-FAN MODEL
$\delta_f = 0°$, $\alpha = 0°$, $\beta_v = 0°$
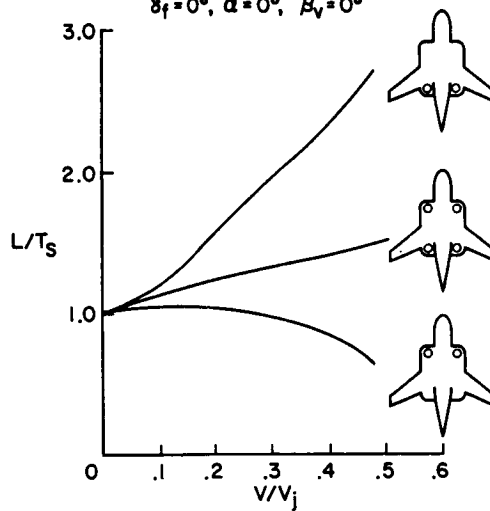
Figure 8

THE LIFT-CRUISE FAN MODEL

Figure 9
L-2698-12

EFFECT OF FRONT-FAN OPERATION ON WING LIFT
$\alpha = 0°$, $\delta_f = 0°$

Figure 10

VARIATION OF LIFT WITH AIRSPEED FOR THE LIFT-CRUISE FAN MODEL

$T = D$, $\alpha = 0^\circ$, $\delta_f = 45^\circ$

Figure 11

THRUST REQUIRED IN LEVEL FLIGHT

$W/S = 100$ LB/FT^2

Figure 12

513
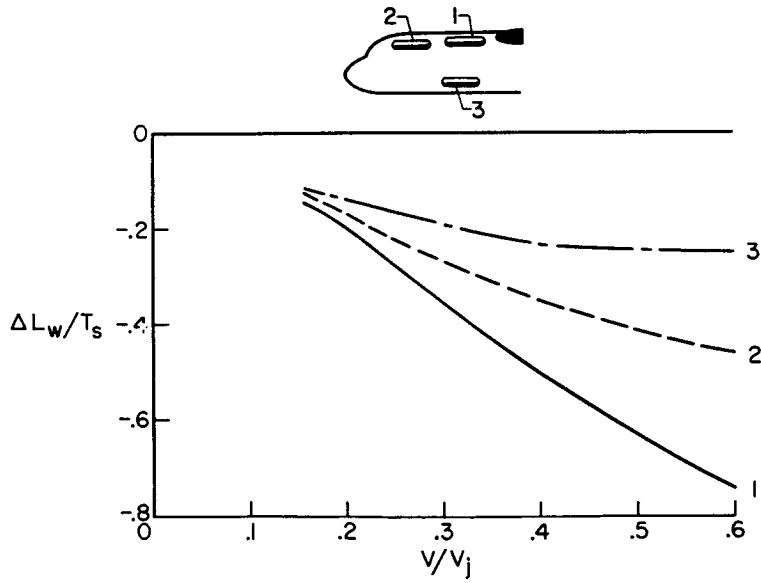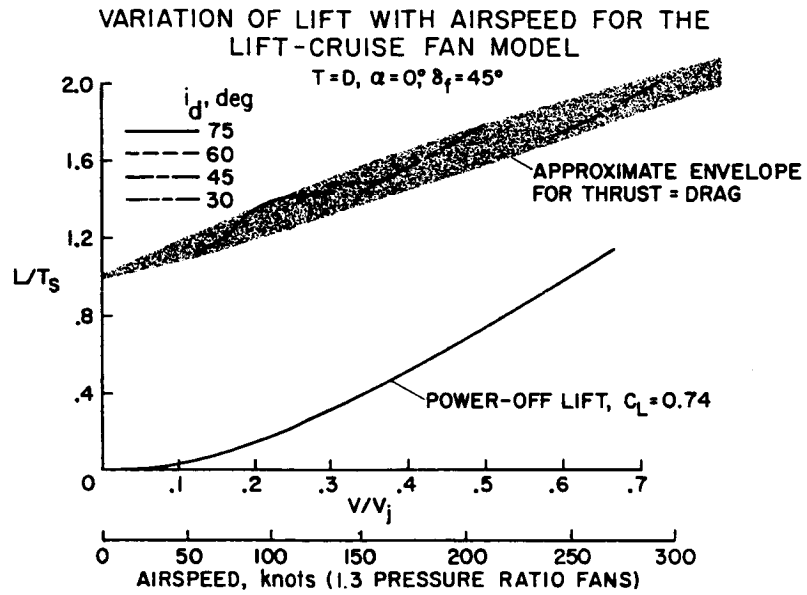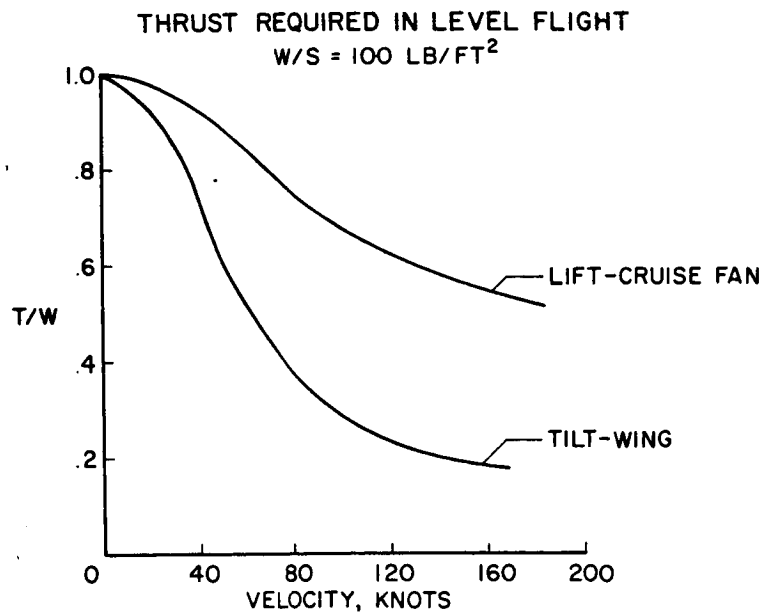
DEFLECTED-SLIPSTREAM CRUISE-FAN CONCEPT

Figure 13

THRUST REQUIRED IN LEVEL FLIGHT
$W/S = 100$ LB/FT^2
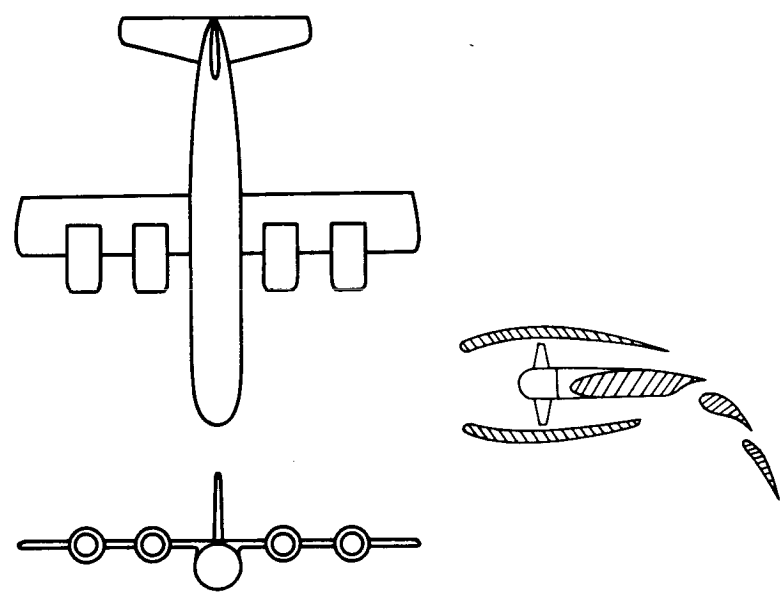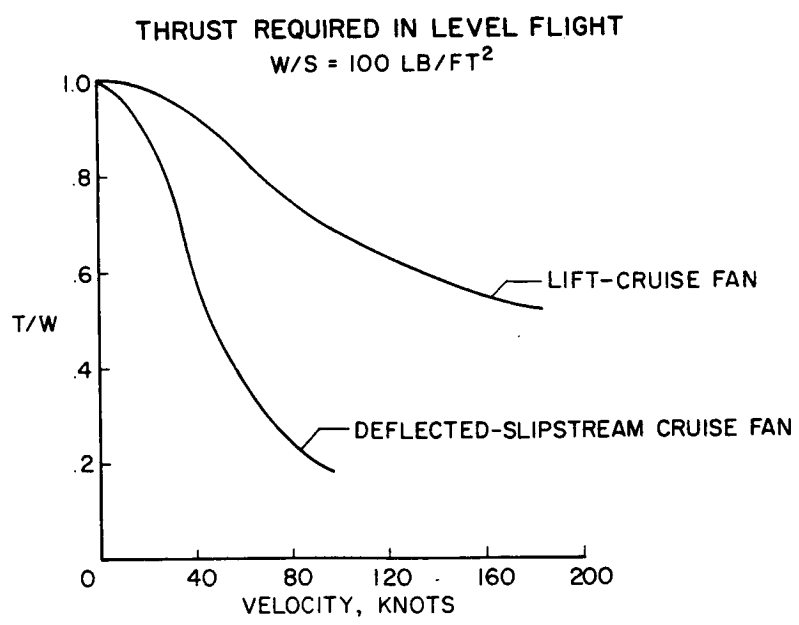
Figure 14

SUBSONIC AERODYNAMIC EFFICIENCY
FIGHTERS; M≈0.8

$$\left(\frac{L}{D}\right)_{max} = \left(\frac{\pi}{4} \frac{b^2}{S_{wet}} \frac{e}{C_f}\right)^{\frac{1}{2}}$$
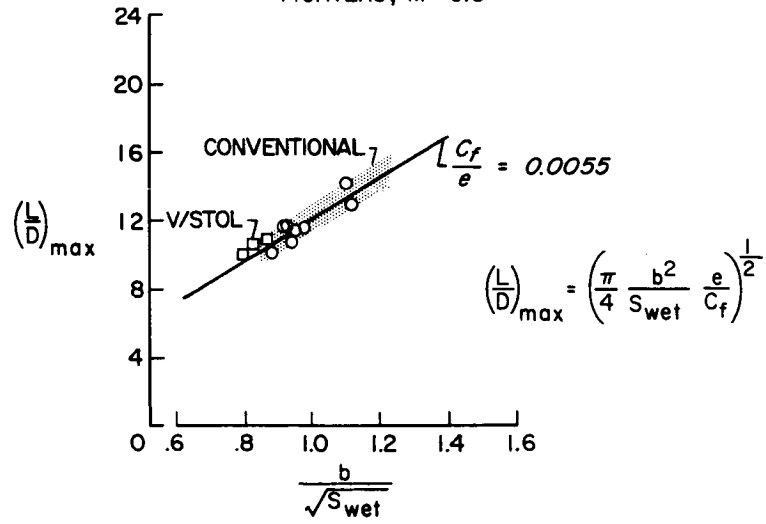
Figure 15

SUBSONIC AERODYNAMIC EFFICIENCY
BOMBERS AND TRANSPORTS; M≈0.8

$$\left(\frac{L}{D}\right)_{max} = \left(\frac{\pi}{4} \frac{b^2}{S_{wet}} \frac{e}{C_f}\right)^{\frac{1}{2}}$$

Figure 16

.515
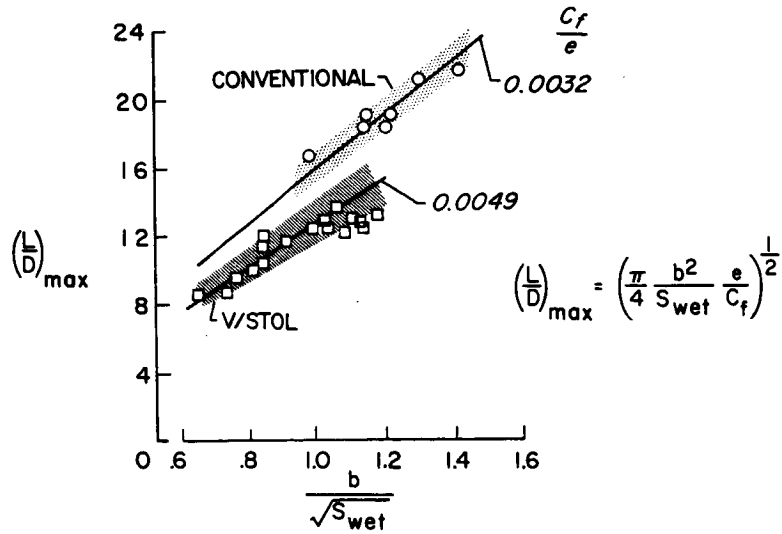
WAVE-DRAG COEFFICIENT
BASED ON FRONTAL AREA; M = 1.2
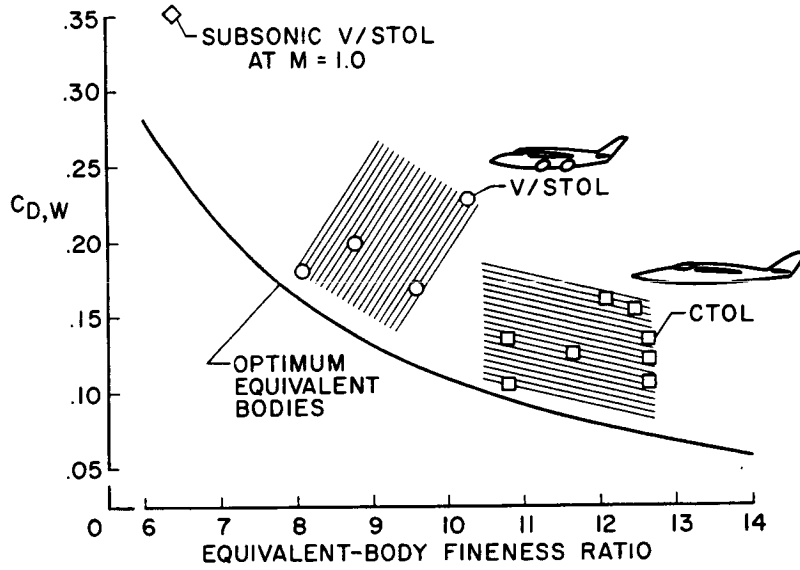
Figure 17

EFFECT OF JET ARRANGEMENT ON BASE LOSS AND JET DECAY

Figure 18

516
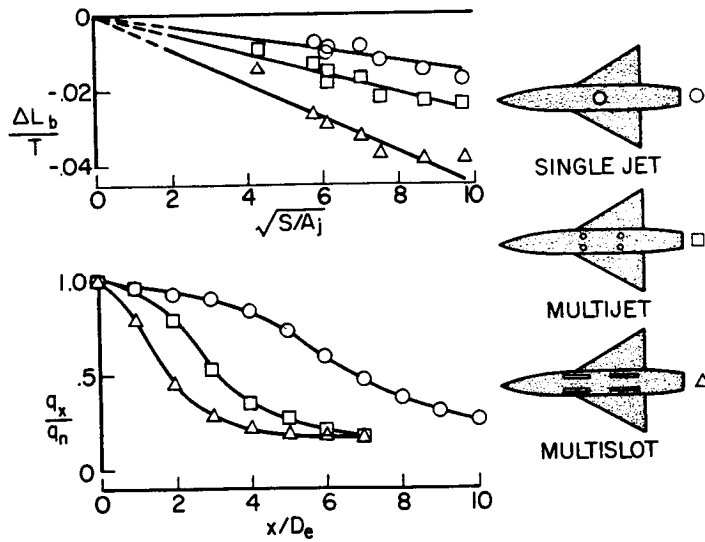
EFFECT OF NOZZLE CONFIGURATION ON JET DECAY
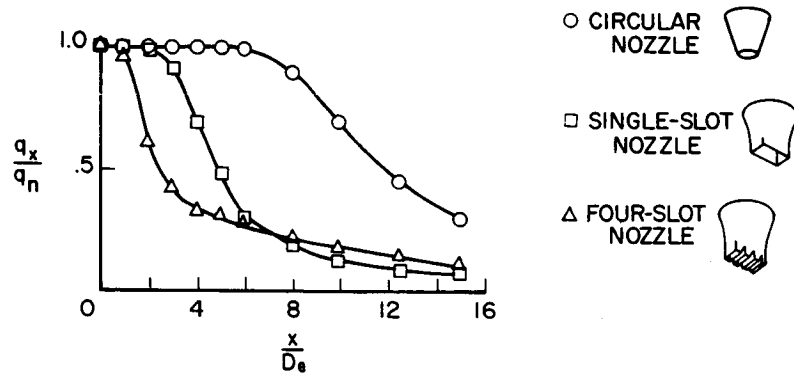
Figure 19

THRUST LOSSES WITH SUPPRESSOR NOZZLES

Figure 20

517
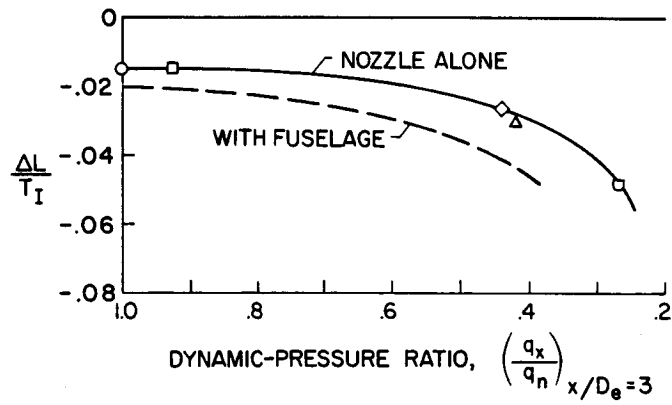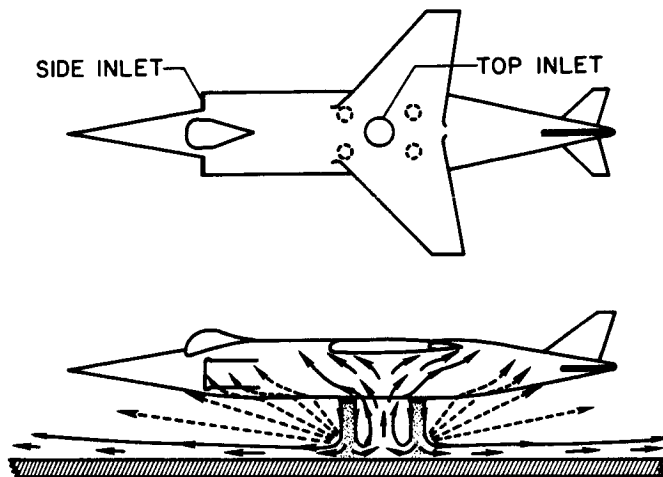
HOT-GAS RECIRCULATION PATTERN
FOUR-NOZZLE CONFIGURATION

SIDE INLET

TOP INLET

Figure 21

INLET TEMPERATURE RISE IN STILL AIR
MULTIPLE NOZZLES ; EGT ≈ 1200° F

TOP INLET

SIDE INLETS

TEMP. RISE, °F

—— LANGLEY MODEL
----- BELL MODEL
—·— NORTH AMERICAN MODEL

$$\frac{\text{NOZZLE HEIGHT}}{\text{EFFECTIVE NOZZLE DIAM}}$$
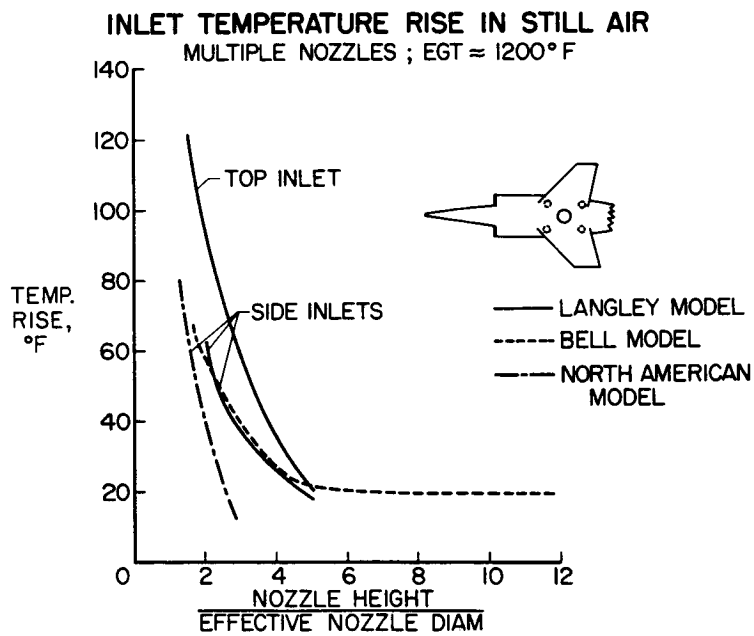
Figure 22

VTOL GROUND EFFECTS AND INGESTION TEST MODEL

INLET LOCATIONS

|←——————— 42.58 ft ———————→|

DEFLECTOR DOORS

WING POSITIONS
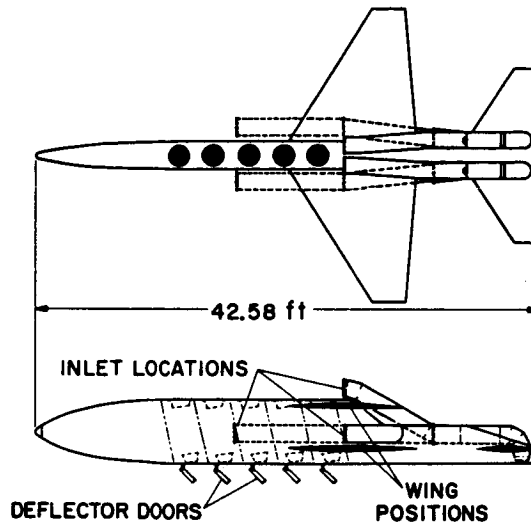
Figure 23

CONFIGURATION HAVING HIGH INGESTION
h/D = 4.5

ENGINE: 1 2 3 4

ENGINE NO. 3 INLET TEMP

200
°F
0

EXHAUST GAS PRESS

20
psi
0

EXHAUST GAS TEMP

1500
°F

0   4   8
TIME, sec
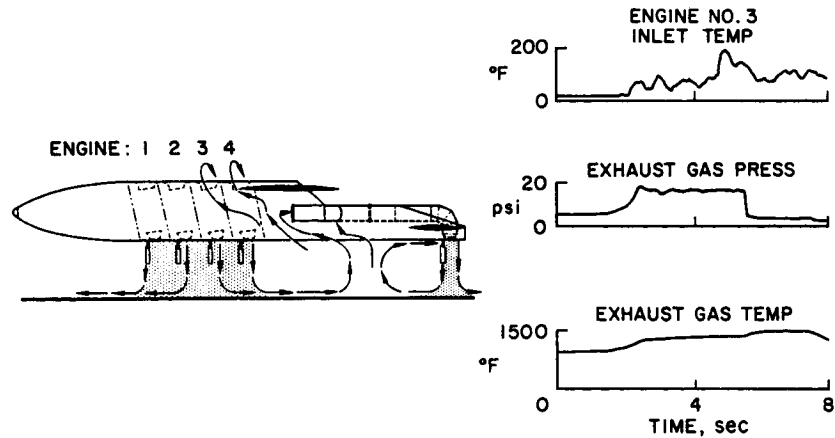
Figure 24

CONFIGURATION HAVING LOW INGESTION
h/D = 4.5

ENGINE: 1 2 3 4

ENGINE NO. 3
INLET TEMP

200
°F
0

EXHAUST GAS PRESS

20
psi
0

EXHAUST GAS TEMP

1500
°F
0   4   8
TIME, sec

Figure 25

EFFECT OF WING PLANFORM
S/A$_j$ = 38

.4

$\frac{\Delta M}{TD_e}$ .2

0

0

$\frac{\Delta L}{T}$ -.2

-.4
0   .1   .2   .3

$$\sqrt{\frac{\rho_\infty V_\infty^2}{\rho_j V_j^2}}$$

Figure 26

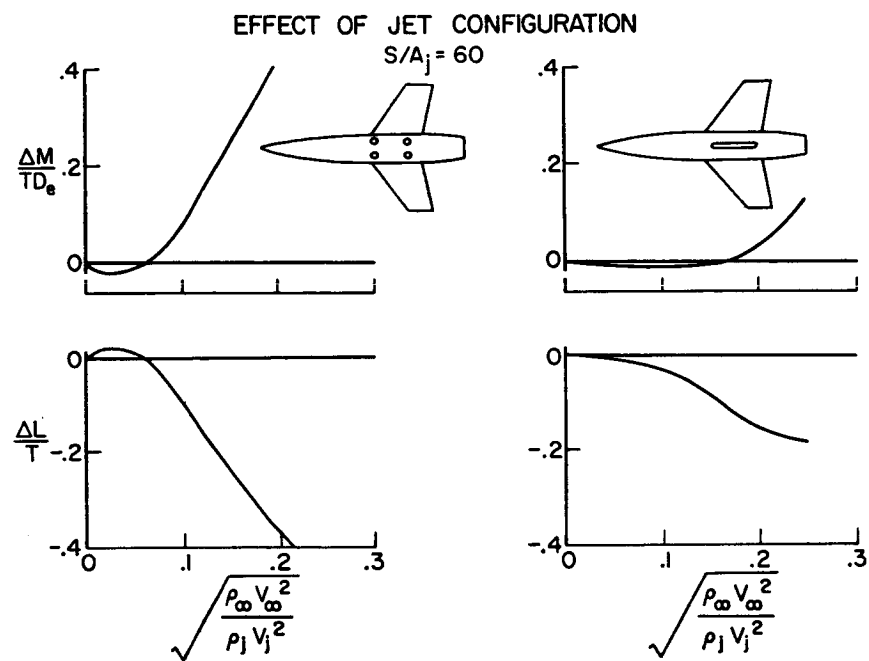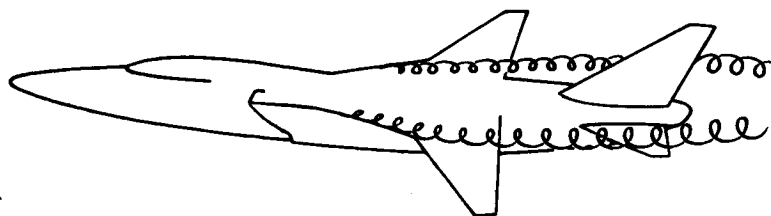## EFFECT OF JET CONFIGURATION

$S/A_j = 60$
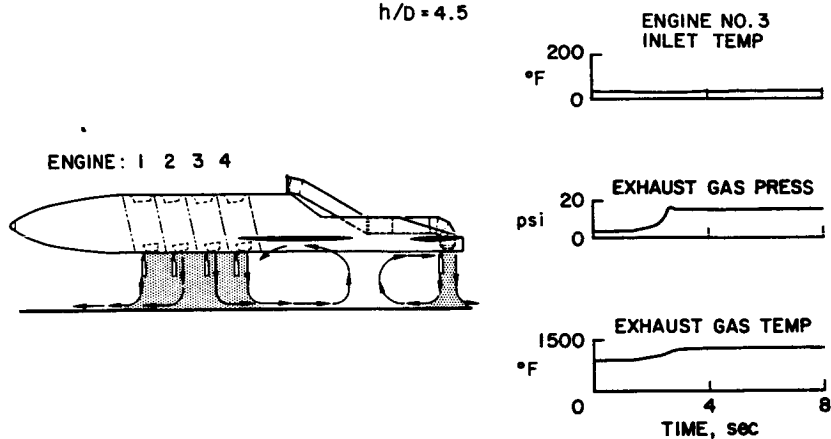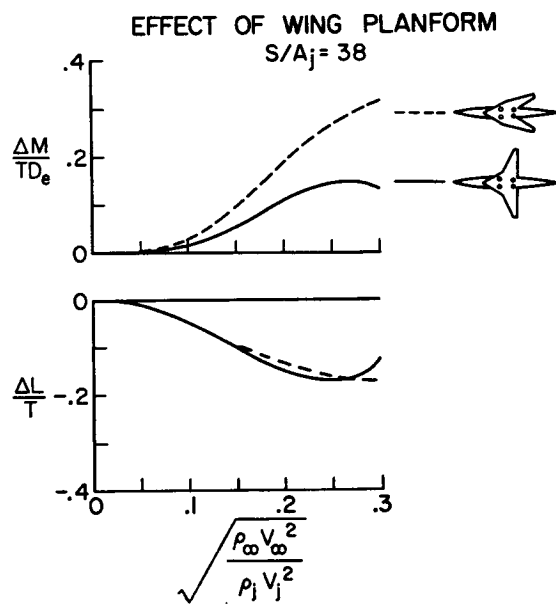
Figure 27

VORTEX PATHS IN CRUISE
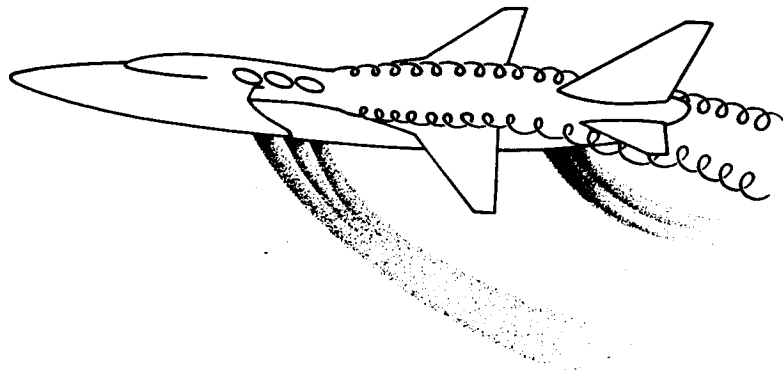

Figure 28

VORTEX PATHS IN TRANSITION FLIGHT

Figure 29